Micro-Cup Architecture for Printing and Coating Asymmetric 2D-Material-Based Solid-State Supercapacitors

Chuanfang (John) Zhang,* René Schneider, Mohammad Jafarpour, Frank Nüesch, Sina Abdolhosseinzadeh, and Jakob Heier*

High energy density micro-supercapacitors (MSCs) are in high demand for miniaturized electronics and microsystems. Research efforts today focus on materials development, applied in the planar interdigitated, symmetric electrode architecture. A novel "cup & core" device architecture that allows for printing of asymmetric devices without the need of accurately positioning the second finger electrode here have been introduced. The bottom electrode is either produced by laser ablation of a blade-coated graphene layer or directly screen-printed with graphene inks to create grids with high aspect ratio walls forming an array of "micro-cups". A quasi-solid-state ionic liquid electrolyte is spray-deposited on the walls; the top electrode material -MXene inks- is then spray-coated to fill the cup structure. The architecture combines the advantages of interdigitated electrodes for facilitated ion-diffusion, which is critical for 2D-material-based energy storage systems by providing vertical interfaces with the layer-by-layer processing of the sandwich geometry. Compared to flat reference devices, volumetric capacitance of printed "micro-cups" MSC increased considerably, while the time constant decreased (by 58%). Importantly, the high energy density (3.99 µWh cm^{-2}) of the "micro-cups" MSC is also superior to other reported MXene and graphene-based MSCs.

1. Introduction

The ever-increasing importance of energy storage devices has greatly stimulated the advancements of novel electrode mate-

C. (John) Zhang
College of Materials Science & Engineering
Sichuan University
Chengdu, Sichuan 610065, P. R. China
E-mail: chuanfang.zhang@scu.edu.cn
C. (John) Zhang, R. Schneider, M. Jafarpour, F. Nüesch,
S. Abdolhosseinzadeh, J. Heier
Laboratory for Functional Polymers
Swiss Federal Laboratories for Materials Science and Technology (Empa)
Überlandstrasse 129, Dübendorf CH-8600, Switzerland
E-mail: jakob.heier@empa.ch
M. Jafarpour, F. Nüesch, S. Abdolhosseinzadeh
Institute of Materials Science and Engineering
Ecole Polytechnique Fedérale de Lausanne (EPFL)
Station 12, Lausanne CH-1015, Switzerland

rials and device architectures.[1] Micro-supercapacitors (MSCs) are known to possess advantages such as long-term cycle life, and fast charging-discharging rate over conventional batteries, but their energy density is much lower.[2–5] Producing MSCs at low cost with higher energy density while maintaining high-rate capacity is important for micro-electronics and microelectromechanical systems (MEMS), but has proven to be quite challenging. Moreover, traditional device fabrication typically involves lengthy procedures such as lithography,[6] masking,[7,8] sacrificial template etching,[9] etc., limiting the scale-up of the MSCs. In other words, developing high-capacitance materials and engineering straightforward, efficient, and scalable device fabrication processes is of great significance and necessity. In comparison, solution processing of functional materials, in particular printing and coating of conductive inks, enable large-scale and cost-efficient fabrication of films/devices, and address the aforementioned challenges.

The design of an efficient supercapacitor requires adapting device architecture and dimensions to the properties of electrode materials and electrolyte or vice versa. Two types of device architectures are currently investigated: conventional sandwich type and in-plane interdigitated electrodes.[10] In the former case, the electrolyte layer is "sandwiched" between two electrode layers. A thin quasi-solid-state electrolyte layer functioning as both separator and ion reservoir is located between two electrodes. Decreasing the thickness of the electrolyte can shorten the ion diffusion distance, resulting in improved capacitance in a compact device. However, ions typically encounter tortuous diffusion paths to reach the active sites for charge storage, whether an electrical double-layer has to be formed or pseudocapacitive redox reactions take place at the surface/sub-surface. For electrodes based on two-dimensional materials with limited pore volume/channels (in the perpendicular direction to the electrical field), the lengthy ion diffusion paths (in the sandwich architecture) negatively impact the rate performance of the device. Furthermore, the only way to increase the energy density of the device is by increasing the electrode thickness which in turn will increase the pathway for ion diffusion, putting a limit on the achievable power.[11]

In the interdigitated coplanar MSCs on the other hand, quasi-solid-state gel electrolytes are usually coated on the surface of the electrodes. Better rate capability and higher power density are expected for higher surface area and shortened ion diffusion path, increasing the thickness can lead to high energy-density devices without an increase in the diffusion length. The interdigitated geometry is thus the currently most researched device architecture in printed devices. Still, the best performance can only be reached by optimizing electrode width and thickness as well as the gap size for each material system individually.[2] As a rule of thumb, increasing the ratio of electrode width to gap width can effectively lower the equivalent series resistance and enhance power density and energy density.[11] For the printed interdigitated devices still, two fundamentally different approaches can be followed, depending if the emphasis is on "small lateral features" or "thick films". High-resolution printing techniques make periodicities in the 25 µm range possible, but do not allow for the deposition of thick films. Techniques like extrusion printing have a lower lateral resolution but allow for the printing of thicker electrodes.[12]

Another differentiation can be made regarding the symmetry of the device: if the two electrodes are made of the same or similar materials, one speaks of a symmetric MSC, if two different materials are used, the device is called an asymmetric MSC. One of the disadvantages of the symmetric configuration is the inherently low operation voltage coupled to the voltage window of the electrode material (e.g., <1.2 V for aqueous electrolytes). Asymmetric MSCs can utilize the voltage window of two materials to maximize the operative voltage of the entire device. Therefore, combining two types of materials (with different charge-storage mechanisms) in an asymmetric device holds the greatest promise in supercapacitor technology.[13] In terms of fabrication, printing high-resolution asymmetric interdigitated electrodes is by far more challenging than printing symmetric devices, as the second electrode material needs to be placed with high accuracy between the fingers of the first electrode.

A further classification can be made with respect to the charge storage mechanism. Electric double-layer MSCs (EDLCs) are frequently fabricated from carbon materials, while pseudocapacitive materials store charge also via fast and reversible faradic reactions.[14] Inks based on carbon nanotubes,[15,16] transition metal oxides,[17,18] 2D layered double hydroxides,[19] transition metal dichalcogenides,[20] graphene,[21,22] etc., have also been reported for printing and coating of high-performance supercapacitors.

One of the most promising EDLC materials for printed MSCs is graphene, not only because of its larger theoretical specific surface area (up to 2630 m^2 g^{-1}), high electronic conductivity, and capacitance of 550 F g^{-1} (if the entire specific surface area is fully utilized),[23] but also for the ease of forming composite materials, which can add pseudocapacitance to the electrode. Symmetric MSCs from graphene have been fabricated by laser scribing (5 mF cm^{-2}),[8] screen printing (1 mF cm^{-2}),[24] inkjet printing (0.27 mF cm^{-2}),[25] gravure printing (37.5 mF cm^{-2}) and other techniques.[26]

Transition metal carbides and nitrides, known as MXenes, are a promising and emerging class of two-dimensional (2D) materials for energy storage applications. MXenes possess an ultra-high volumetric specific capacitance via the interaction between the surface functional groups and ions in the electrolyte.[27] Few-layer MXene flakes can be formulated into viscous delaminated MXene inks for inkjet printing,[28,29] extrusion printing,[30] stamping,[31] blade coating,[32,33] etc. However, due to the relatively low delamination yield, the majority of solids are typically discarded after collecting the delaminated MXene,[34,35] raising the fabrication cost where applications rely on delaminated flakes. But we have previously reported that multilayer sediments of MXenes can be processed into printable inks by adding small amounts of single-layer flakes. Despite the high sediment content, these inks proved to be an excellent choice for screen-printing of coplanar interdigitated MSCs.[36] Nevertheless, the large finger gap coupled with the aqueous gel electrolyte limit the device capacitance at high rates and voltage window, respectively, leading to compromised energy density and power density in the as-achieved MSCs.

The major concern of the asymmetric interdigitated (planar) electrode configuration relates with the need to precisely position the second finger electrode between the first finger electrodes, which poses serious restrictions to the lateral resolution that can be achieved with printing techniques. High-precision printers demonstrate overprint accuracies in the range of 10 µm, when thinking of roll-to-roll techniques that range easily exceeds 100 µm. There is thus a strong need to find an architecture for asymmetric devices that can be printed.

We here introduce a new device architecture, which is based on a "cup & core" structure designed to support asymmetric devices and eliminate the need of precise overprinting. The "cup & core" configuration minimizes the inter-electrode distance while avoiding short circuits. We demonstrate the concept with graphene "micro-cups" which are fabricated by both, laser scribing and printing. A layer of quasi-solid-state ionic liquid electrolyte (IL-EL) is spray-coated on top of the micro-cups, and finally, the cups are filled with MXene sediment ink. Both strategies showed better performance over the conventional flat layer architecture in terms of volumetric capacitance and time constant. This study may lead the way to large-scale and low-cost production of advanced solid-state MSCs for next-generation electronics.

2. Results and Discussions

The ion movement and the accessible electrode surface of the cup-core structure is compared with the sandwich architecture shown in **Figure 1**. Unlike conventional sandwiched or interdigitated MSCs, which typically suffer from lengthy ion diffusion paths and large electrode gaps, respectively, micro-cups MSCs (µcup-MSCs) efficiently combine the advantages of both architectures (sandwiched and interdigitated) by creating a graphene electrode grid structure which then forms an array of three-dimensional µcups.

On a larger scale and from a manufacturing perspective, the device resembles a sandwich structure, whereas locally an interdigitated structure is obtained with electrolyte and top electrode filling the cups. As such, the distance between two electrodes is decreased, and the diffusion of the ions is facilitated, due to the parallel orientation of the nanosheets and diffusion direction.
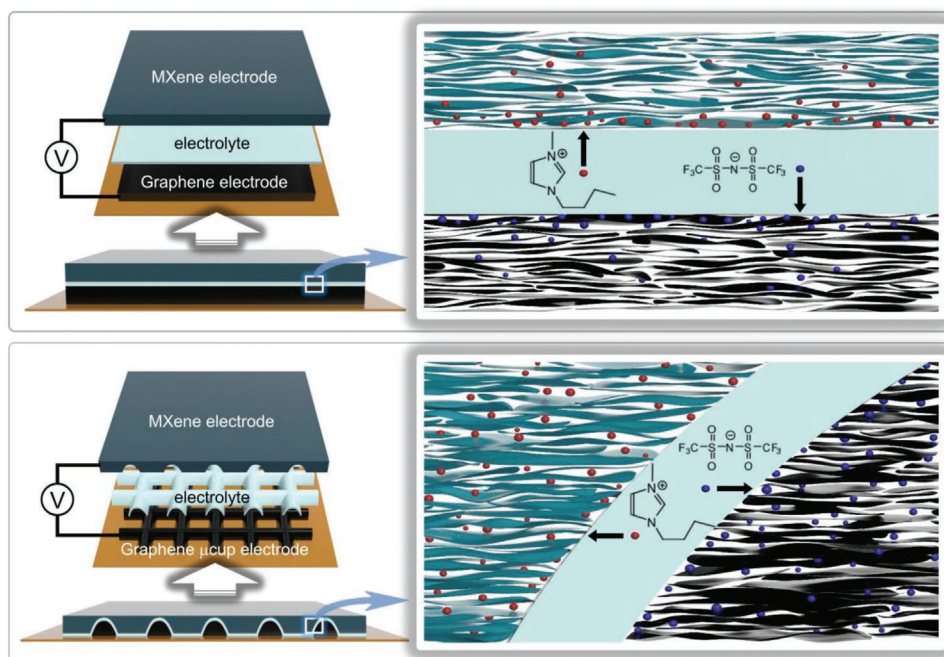
**ADVANCED
SCIENCE NEWS**

www.advancedsciencenews.com

**NANO · MICRO
small**

www.small-journal.com

Figure 1. Schematic illustration showing advantages of µcup-MSCs compared to a conventional flat MSC. µcup-MSCs facilitate the ion diffusion kinetics, increasing the utilization of active materials and thus enhancing the charge storage properties at a smaller electrolyte thickness. Consequently, the improved specific capacitance coupled with the wider voltage window from the IL electrolyte ensures much higher energy density and power density in the µcup-MSCs.

2.1. Device Fabrication

µcup structured graphene electrodes were fabricated by either blade-coating and subsequent Laser-scribing (sample names starting with L), or a screen-printing process (samples starting with P), as sketched in **Figure 2**A. In the case of blade-coating and Laser scribing, the graphene ink, optimized for blade coating was coated on glass substrates and dried at room temperature.

After subsequent thermal annealing at 300 °C, graphene films were achieved with abundant voids formed as a result of the burning of the ethyl cellulose binder present in the ink. The Raman spectrum (Figure S1, Supporting Information) of the printed film exhibits the typical peaks of liquid-phase exfoliated graphene with D and G bands at 1334 and 1578 cm^{-1}. The G peak is attributed to the E_{2g} optical phonon of graphene, while the D band is originated by breathing modes of six-atom rings and requires a defect for its activation.[37] The relative intensity of the D peak to G peak ($I_{(D)}/I_{(G)}$), which is a widely accepted criterion for evaluation of the defects in graphene, is in the similar range (≈0.477) as the previous reports.[37] Using ($I_{(D)}/I_{(G)}$), the defect density of the graphene can be estimated[38] to be ≈5.3 × 10^{10} defects/cm^2. The high fraction of voids coupled with defects in the final graphene electrode may influence the charge storage properties, as will be discussed below.

The graphene film was then structured by laser-scribing. The nanosecond UV laser has a beam diameter of 20 µm and can readily ablate µcups in the 100 µm range as demonstrated in Figure 2C,E. Each µcup has dimensions of roughly 200 µm. Figure 2C shows the topography of the laser-scribed graphene µcup arrays (Sample L7W) obtained with a confocal micro-scope, indicating a smooth surface with identical µcups. The height profile along the dashed line in Figure 2C implies that the µcups are ≈30 µm in depth. To optimize the Graphene electrode geometry, the µcup-distance was varied resulting in different wall width, as shown in Figure 2E (samples denoted with L#T, M, or W for thin, medium, and wide walls). A wall width < 65 µm could not be achieved without a substantial damage of the Graphene walls. The layer thicknesses of the Laser-scribed samples, as well as the corresponding resistivity values are shown in Figure 2F. The resistivity values are low enough to use the grids not only as an electrode, but also as the current collector. The values do not show a large variation for the different grid geometries, which shows that the grids are quite comparable.

The real benefit of the novel µcup electrode configuration lies in the potential to print asymmetric MSCs, as only the bottom electrode requires the printing of lateral structural features. Compared to the abovementioned 2-step procedure of coating and laser-scribing, screen printing simplifies the µcup fabrication to only one step. To ensure efficient screen printing, inks are usually tuned to yield suitable rheological properties. A very high solid content ink was formulated to enable printing thick layers on each print pass. Additionally, the high viscosity of the ink ensures that the shape of the printed structures is maintained after removing the shear force. In terms of rheological properties, the storage modulus in the used graphene inks is lower than the loss modulus at all strains (Figure 2D). The ink exhibits non-Newtonian characteristics and shear-thinning (pseudoplasticity) behavior with an apparent viscosity up to 100 Pa·s (Figure S2, Supporting Information).
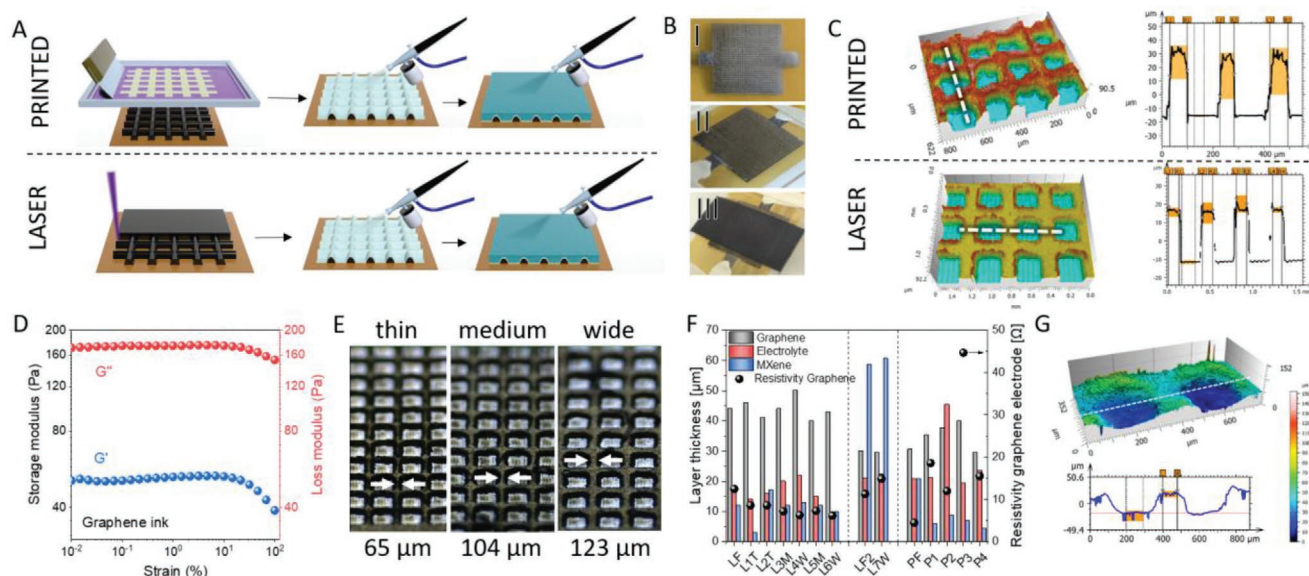
Figure 2. Fabrication and Characterization of the solid-state device. A) Schematic of the fabrication process of the μcup electrodes by screen-printing or blade coating and subsequent laser scribing. Followed by spray coating of the Electrolyte layer and the top electrode. B) Photographs of the printed μcup electrode (I; P3), μcup electrode and electrolyte layer (II), and the final device including the MXene top electrode (III). C) Topological images of the printed (P3) and laser-scribed (L7W) graphene μcups and the corresponding height profile along the grids, showing the surface of graphene μcups and even thickness of the grids. D) Storage modulus (G′) and loss modulus (G″) of graphene ink. E) Micrographs of the Laser scribed cup-electrodes with various wall width. F) Layer thicknesses and resistivity of the μcup-graphene electrodes for all devices; thicknesses were measured by confocal microscopy or SEM cross-section. G) Topological image after spraying the quasi-solid-state IL electrolyte on the graphene μcups (top) and the corresponding height profile along the dashed line (bottom). The image shows that the μcup structure is maintained after spraying of the EL layer.

Aside from the materials, the μcup geometry has an impact on device performance. This can easily be demonstrated by varying the periodicity of the cup structures and the width of the μcup walls and evaluating the device's charge storage properties. Figure 2B-I shows an optical image of an as-printed graphene μcups/grid, while microscope images of 4 different grids with their topography and height profiles are shown in Supplementary Figures S3 and S4, Supporting Information. Compared to the blade-coated and Laser- scribed samples, the screen-printed samples show textured surfaces which are attributed to ink drag-out upon lifting the mesh off the substrate, which is due to the insufficient leveling of the ink after deposition (Figures 2C,S4, Supporting Information).[36] The μcup depths are determined by confocal microscopy and averaging over the height profiles of the μcup walls (Figures 2C-F, S4, Supporting Information). In screen printing the printed layer thickness (μcup depth) is determined by the mesh and emulsion thickness, all 4 different grids show a comparable μcup depth between 30 and 40 μm (Figure 2F). The different μcup size and wall thickness of the 4 different grids also affect the graphene: void ratio per unit volume and the overall resistivity of each grid, as shown in Figures S5 and S6, Supporting Information, respectively. After fabrication of the graphene μcup electrode, a quasi-solid-state ionic liquid electrolyte (poly(vinylidenefluoride-co-hexafluoropropylene) (PVDF-HFP) / 1-butyl-3-methylimidazolium bis(trifluoromethylsulfonyl)imide (BMIMTFSI) / ethylenecarbonate (EC)) was applied by spray coating or dip-coating from acetone solution onto the structured graphene electrode (Figure 2B II). Both methods work well

and deliver comparable electrolyte films. The electrolyte has high ionic conductivity, a wide voltage operation window, and has shown good performance in carbon-based supercapacitors.[39] The topological image of the electrode/electrolyte stack (Figure 2G), as well as the SEM images (**Figure 3**, Supplementary Figure S7) indicate a relatively even surface after depositing the electrolyte. From the height profile, one can conclude that the μcup architecture is well conserved with the quasi-solid electrolyte following the underlying topography. The cross-sectional SEM images in Figure 3 reveal that the IL electrolyte layer, which also acts as the separator, well isolates two electrodes from short circuit. Figure 3 also suggests the quasi-solid-state electrolyte thickness of ≈9–16 μm. This is a typical dimension for a sandwich structure, but is a very challenging task for printed interdigitated electrodes to realize such a narrow electrode gap.

To complete the device, MXene ink was spray coated on the top of the Graphene/Electrolyte stack. The smooth film follows the topography of the underlying layer, while the MXene sheets stack in a layered structure (see Figure 3) The cross-sectional SEM image of the graphene electrode/electrolyte interface also shows the horizontal alignment of the graphene flakes, which enables an unhindered access of the electrolyte ions from the side to intercalate between the graphene sheets (Figure 3F). The SEM-cross-sections were prepared by freezing the sample in liquid Nitrogen followed by breaking the sample. This harsh procedure can lead to deformation and/or drag-out of material, as well as delamination due to the shrinking of materials upon freezing. Delaminated areas are indicated with red arrows in Figure 3B,C,E.
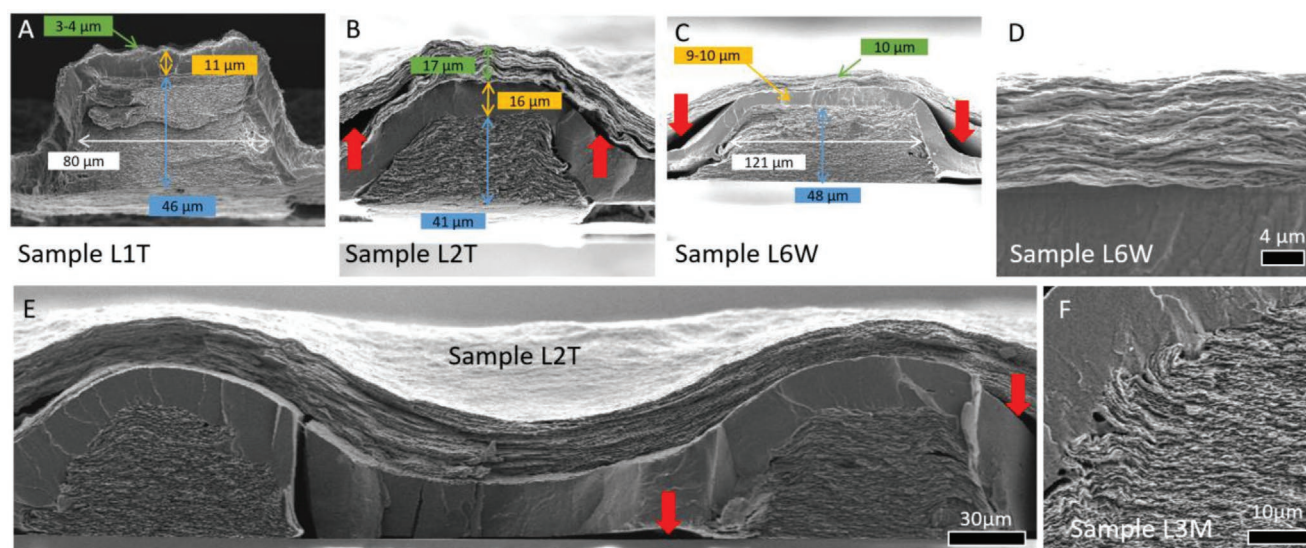
ADVANCED
SCIENCE NEWS
www.advancedsciencenews.com

NANO · MICRO
small
www.small-journal.com

Figure 3. SEM cross-section of selected devices. A,B,E) Dimensions of the µcups and the different layers for thin walled samples and a wide wall sample C,D) Close-up of the Electrolyte-MXene interface, showing the horizontal alignment of the MXene flakes. F) Close- up of the Electrolyte-Graphene interface, showing the horizontal alignment of the MXene flakes. Delaminated areas, caused by freezing in liquid N_2 are indicated with red arrows in (B,C,E).

2.2. Electrochemical Characterizations of µcup-MSCs

The electrochemical charge storage properties of the µcup-graphene / Il-EL/ MXene (µcup-MSC) devices were investigated and compared to that of a conventional sandwiched device with a nonstructured graphene electrode (flat-MSC). Typically MSC performance is evaluated by areal capacitance (F cm^{-2}), as the devices are usually very thin and the mass is comparatively small. The laser-scribed µcup- as well as the flat devices exhibit a considerable thickness, so that mass cannot be neglected. Thus, we believe that the specific capacitance (F g^{-1}) or volumetric capacitance (F cm^{-3}) are the more important metrics, because weight and volume play a crucial role in many applications, e.g., mobile devices or airplanes. This work specifically investigates the effect of the structural morphology and the occupied volume of the bottom electrode. As these can be accurately measured using confocal microscopy (Figure 2C and S4, Supporting Information) the volumetric capacitance (F cm^{-3}) will be used to compare the MSCs. For completeness, we also show the areal capacitances in the Supporting Information calculated on the basis of device area including the "dead"-area of the µcup bottom (for the main devices: Figure S19, Supporting Information). It is quite challenging to assign a fair comparison of the charge storage properties of the solid-state MSCs. Due to the usage of a quasi-solid electrolyte, it was impossible to evaluate the single electrode properties by a standard three-electrode test. Instead, the performance of the whole device was determined by cyclic voltammetry (CV) as well as by Galvanostatic charging-discharging (GCD) measurements. The evaluation of the capacitance per electrode is not straightforward, to be able to make a statement, a charge balance of the 2 electrodes was assumed. The volumetric capacitance (C/V) was calculated, as described in the SI, using the graphene electrode volume (V) as this is the electrode of interest.

It was found that the Coulombic efficiency (CE) reaches >99 only when the cutting voltage is kept below 1.5 V. For instance, when the device was measured at 0–2 V, a sharp tail can be found in the region between 1.6 and 2 V (Figure S8, Supporting Information). While this voltage window (0-1.5 V) is much wider compared to the 0.5 V observed in symmetric MXene MSCs,[7,31,36] or 1 V in asymmetric devices,[40,41] it's considerably lower than the typically reported values such as 3 V in MXene supercapacitors based on an IL electrolyte.[42,43] Possible reasons include but are not limited to: the residues formed due to the thermal annealing of the graphene electrode react adversely with the IL at high voltage, leading to a lower device CE beyond 1.5 V, and second, the mismatched mass of the two electrodes results in charge polarization. We expect a much higher voltage window in the MSCs by addressing these two issues, i.e., employing additive-free graphene inks to fabricate the electrode, and/or optimizing the mass ratio of two electrodes. However, this is not trivial as described above.

To evaluate the influence of the top electrode thickness, one laser-scribed device was prepared with a thin MXene layer (thickness 3–4 µm; device L1T), and its charge storage properties was measured by CV. Afterward another MXene layer was spray-coated, the device was re-measured and the coating/measurement cycle was repeated. By using the same device, the influence of other parameters than the MXene thickness can be excluded. **Figure 4**A shows the volumetric capacitance at different scan rates for increasing MXene film thickness. By plotting C/V at 20 mV s^{-1} versus the MXene film thickness, a saturation at ≈ 10–15 µm can observe. Beyond that, increasing the thickness of the MXene electrode does not help to gain a higher performance as indicted by the nearly identical CV curves for the MXene layer thickness of 15 µm and 17 µm (Figure S9, Supporting Information).

In a capacitor, the distance or channel width between the two electrodes plays a crucial role and should be as thin as possible. In a sandwich-type device, the electrolyte layer determines the electrode distance and separates the two electrodes from electrical short circuit. In the present µcup-case it is much more
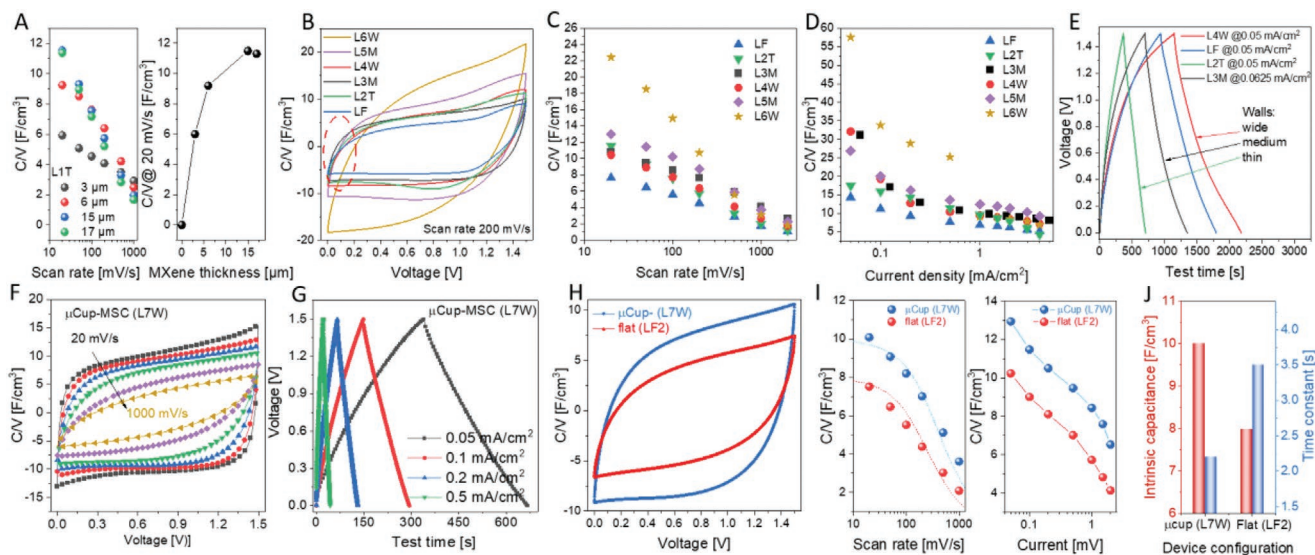
Figure 4. Electrochemical Characterization. A) Volumetric capacitance (*C/V*) at different scan rates for an increasing thickness of MXene top electrode. A saturation at ≈ 10–15 µm can be observed at a low scan rate. B) Normalized CVs for Laser scribed devices at a scan rate of 200 mV s⁻¹. C,D) Comparison of volumetric capacitance of µcup-MSCs and flat-MSCs calculated from CVs and GCDs, respectively. E) GCD curves of laser scribed µcup-MSC at comparable current density as a function of the µcup-wall size. F) Normalized CVs for L7W at different scan rates, as well as G) GCD curves at low current densities. H) Normalized CV comparison of µcup-MSC (L7W) and flat-MSC (LF2) at 200 mV s⁻¹. I) Comparison of volumetric capacitance of µcup-MSC (L7W) and flat-MSC (LF2) calculated from CVs and GCDs, respectively. J) Intrinsic volumetric capacitance and time constant of µcup-MSC (L7W) and flat-MSC (LF2), obtained from fitting using the Equation (1).

challenging to coat the bottom electrode compared to a flat device, as the topography is much more difficult. Thus it was not possible to coat an electrolyte layer with thickness << 10 µm, which showed a sufficient electrode separation. Consequently most of the devices had an electrolyte layer with > 10 µm as shown in Figure 2F. A thin electrolyte sample (L6W) shows highest capacitance of all investigated samples (see Figure 4B,C,D). As the MXene top electrode, as well as the Graphene electrode are comparable to the other devices, the thickness of the electrolyte layer is suspected to cause this improvement on the performance. The CV shows strong deviation from the quasi-rectangular shape, already at an intermediate scan range of 200 mV s⁻¹ which is inferior to the other devices (Figure 4B). Usually, this effect can only be seen at higher scan rates, when the ion diffusion time is too slow to follow the scan rate. GCD measurements at low current densities also confirm a high *C/V* where sample L6W showed much longer charge/discharge times than the comparable sample L4W (See Figure S10, Supporting Information). In Figure 4C,E it is also evident that the *C/V* drops much faster when going to higher scan rates (or higher current densities) compared to the other samples. This also indicates that the device with a thin electrolyte layer shows declined and slow power handling. This result suggests, that it is a trade-off between high capacitance and fast response and that no general recommendation is possible.

Devices L2T, L3M, and L4W as well as the flat one (LF) show similar layer thicknesses and therefore are highly comparable and suitable to investigate the influence of the µcup wall width. As shown in Figure 2E the width decreases from 123 µm to 104 µm to 65 µm for L4W, L3M, and L2T, respectively. As the size of the cups is constant, the Graphene Volume in the µcup-

electrode decreases accordingly. Figure 4B shows the normalized cyclic voltammograms (CVs) for various µcup-MSCs at 200 mV s⁻¹ scan rate. It is evident, that the flat device encloses a significantly smaller area than the µcup-devices, which indicates a lower volumetric capacitance and lower charge-storage performance. By comparing the encircled area in Figure 4B for the abovementioned devices small differences are visible. The µcup-MSCs require less time to stabilize the current, indicative of improved power handling compared to the flat device. Figure 4C shows the volumetric capacitance obtained from CV scans at different scan rates and also no clear trend is visible. This suggests that the wall thickness of the µcups has no or only minor influence on the device performance within the investigated scan rates. The volumetric capacitance obtained from GCD (Figure 4D) experiments shows similar behavior: The improvement of the µcup-samples is even more pronounced and reaches more than double *C/V* (for L3M at low current density) compared to the flat device. At closer look at the GCD curves, the influence of the wall width is visible: Figure 4F reveals the time needed to run a charge/discharge cycle of the devices at low current densities (0.05 mA cm⁻²). The charge/discharge times decrease and thus the capacitance decreases as the walls become thinner. Note, that the current density is calculated from the device area, which also includes the "dead" area of the µcup bottom, which doesn't allow a fair comparison by GCD curves. Nevertheless, the wide walls device (L4W) shows better performance than the flat (LF) one. Additional data, which shows the decreasing test time for thinner wall widths for 0.5 mA cm⁻² and 2 mA cm⁻² is shown in Figure S11, Supporting Information.

In order to gain further insight a device with quasi-rectangular CVs and its corresponding flat device (L7W, LF2) was chosen for a more detailed electrochemical characterization.

**ADVANCED
SCIENCE NEWS**

www.advancedsciencenews.com

**NANO · MICRO
small**

www.small-journal.com

Figure 4F shows these cyclic voltammograms (CVs) of a μcup-MSC at different scan rates. A capacitive charge-storage behavior is observed, as evidenced by the quasi-rectangular CVs ranging from 20 mV s⁻¹ to 1000 mV s⁻¹. GCD also confirms the good power handling property and highly capacitive behavior in μcup-MSCs (Figure 4G), as linear, symmetric curves are found in the absence of any plateaus or apparent IR drops even at 2 mA/cm² (Figure S12, Supporting Information). In contrast, the flat-MSC displays an inferior rate behavior, as seen from the nonrectangular CV shapes starting from 200 mV s⁻¹ (Figure S13, Supporting Information).

By comparing the normalized CVs of two MSCs at 200 mV s⁻¹ (Figure 4H), it appears that the μcup-MSC requires less time to stabilize the current, indicative of improved power handling. Indeed, the volumetric capacitance of μcup-MSCs is much higher than that of the flat-MSC, as confirmed by the CV measurements (Figure 4I). The volumetric capacitances obtained from GCD tests show the same trend. Such an improved rate response is also revealed by the capacitance retention (50.4% in μcup-MSC versus 40.4% in the flat device when elevating the current density 40-fold, Figure S14, Supporting Information). Moreover, being able to fit the capacitance versus scan rate using an empirical equation (Figure 4I):

$$\frac{C}{V} = C_V \left[1 - \frac{\nu\tau}{\Delta V} \left(1 - e^{-\frac{\Delta V}{\nu\tau}} \right) \right] \tag{1}$$

where $\tau = R_{ESR}C$ is the time constant, ΔV is the voltage window (1.5 V), ν is the scan rate and C_V is the intrinsic volumetric

capacitance, is ideally achieved when the electron/ion diffusion limitations across the whole electrodes are eliminated.[44] Although this model simplifies the complex electrochemical behavior of the electrode, it still yields valuable insights into the overall behavior of the thin film electrodes.[45] As seen in Figure 4J, the μcup-MSC possesses a lower τ (2.2 s versus 3.5 s) compared to those of flat-MSC, indicating an improved ion diffusion kinetics, leading to enhanced power handling.

2.3. Electrochemical Characterizations of Screen Printed μcup-MSCs

As described above, the screen-printed samples show textured surfaces and stronger variation in width and height compared to the Laser-scribed samples. This makes it very difficult to attribute the different charge storage properties to the individual grid structures. The μcup design (wall width and cup size) was optimized to improve the charge storage properties of resultant printed μcup-MSCs: As **Figure 5**D suggests, a high volumetric capacitance can be reached for sample P1, where the walls are thin and the free volume of the structured electrode is large. Generally, the findings are very similar to the Laser-scribed devices: The μcup-MSCs showcase pseudocapacitive behavior and high-rate handling, as seen for from the rectangular CV shape (Figure 5A) and symmetric linear GCD curves (Figure 5B) for device P1 (additional data in Figure S15, Supporting Information).

In contrast, the flat-MSC displays resistive CVs at scan rates beyond 200 mV s⁻¹ and smaller charging-discharging
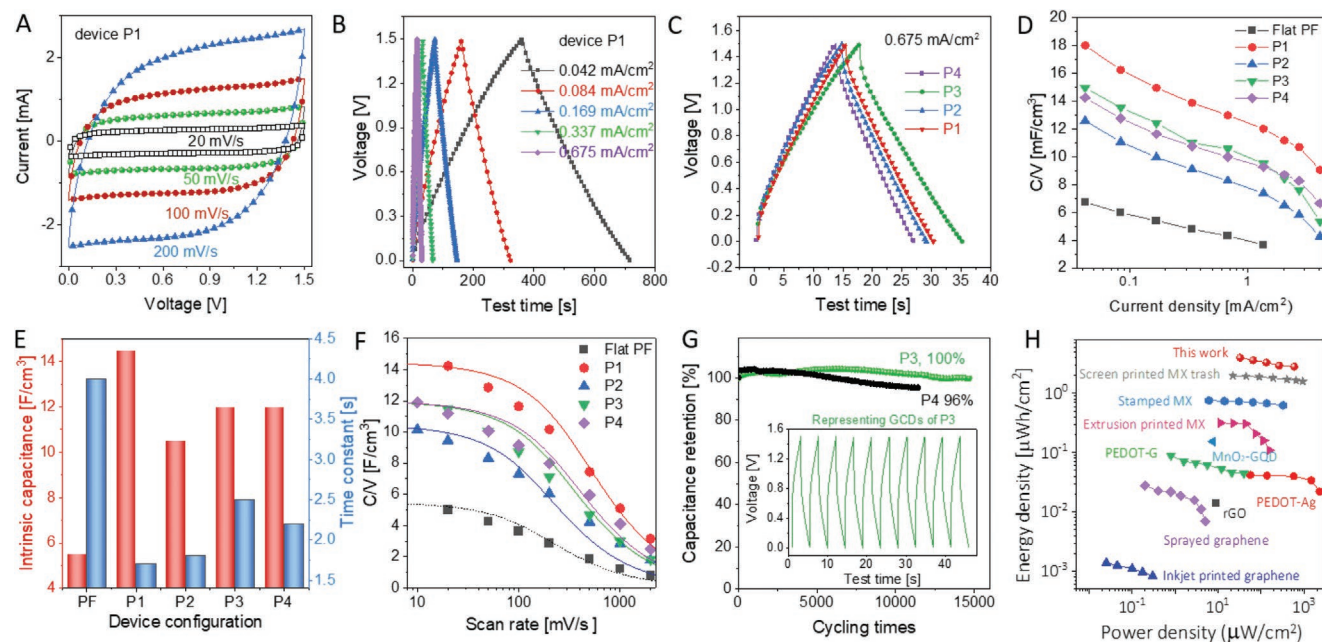

Figure 5. Electrochemical Characterization of printed devices. CV curves A) GCD profiles B) of screen-printed P1 μcup-MSCs at different scan rates. GCD profiles C) and volumetric capacitance D) of MSCs for different μcup sizes and the flat device (PF). E) Intrinsic volumetric capacitance and time constant for different μcup-MSCs in comparison to those of flat device configuration obtained from fitting data in Figure 5F using the Equation 1). F) Volumetric capacitance obtained from CV measurements of MSCs including flat-MSC. G) Long-term cycling performance of P3 and P4, inset shows the typical GCD curves during cycling. Ragone plot comparison of this work (P3) to other MSC systems, showing the advantages of employing the μcup-MSCs in achieving both high energy density and power density (H).

ADVANCED
SCIENCE NEWS
www.advancedsciencenews.com

NANO · MICRO
small
www.small-journal.com

times at similar current densities, suggesting lower volumetric capacitance and inferior rate performance (Figure S16, Supporting Information). CV and GCD curves of the printed µcup-MSCs are summarized in Figure S17, Supporting Information. CVs at 20 mV s^{-1} are compared for the printed- and flat-MSCs (Figure S18, Supporting Information), and GCDs at 0.675 mA cm^{-2} are shown for the printed MSCs (Figure 5C). Based on the GCD measurements, the volumetric capacitance in the P1 device reaches 18 F cm^{-3} and maintains 9.1 F cm^{-3} even when increasing the current density 96-fold (Figure 5D). In contrast, despite the flat-MSC (PF) having a much thicker MXene electrode, the capacitance decreases from 6.7 to 3.7 F cm^{-3} (capacitance retention of 55% as increasing the current density by 32-fold), suggesting a poor utilization of active material in the flat device architecture. By fitting the capacitance versus scan rate (Figure 5F) according to the abovementioned Equation (1), a maximum C_V and a minimum τ for P1 are observed. This confirms, that the grid morphology (e.g., wall width and height; cup density) plays a crucial role in the device performance as already shown by the Laser scribed devices. Compared to the printed µcup-MSCs, the flat-MSC exhibits the lowest C_V and the highest τ, demonstrating the advantages of the µcups with respect to the enhanced volumetric capacitance and power handling (Figure 5E).

The GCD long-term cycling tests of two typical printed µcup-MSCs were performed at 2.7 mA cm^{-2}, with results shown in Figure 5G. While the P4 device decays by 4% of its initial capacitance after cycling 11410 times, the P3 device maintains its initial capacitance without any capacitance decay after charging-discharging 14665 times. Representing GCDs of P3 reveal well-defined symmetric quasi-linear curves upon cycling (inset of Figure 5G), suggesting highly reversible, pseudocapacitive behavior without parasitic reactions.

As mentioned above, the specific- or volumetric capacitance was chosen to ensure a fair comparison between the µcup-MSC and the flat-MSC. To enable a comparison with other devices the energy density and power density was calculated based on the areal capacitance per device. It is worth mentioning that many MXene-based MSCs show higher energy- and power density and therefore outperform the µcup-MSCs.[46] Both, the material, as well as the device optimization to gain champion-performance was beyond the scope of this work. The calculated energy density of the printed µcup-MSCs (P3) reaches as high as 3.99 µWh cm^{-2} at 32.6 µW cm^{-2}, and still maintains 2.82 µWh cm^{-2} at a maximum power density of 588.9 µW cm^{-2}. The energy density is much higher than in our previously reported screen-printed MSCs based on MXene sediment inks,[36] inkjet- or extrusion-printed all-MXene MSCs,[30] and stamped, interdigitated coplanar MXene MSCs.[31] The benefit of the unique device configuration, as well as the utilization of quasi-solid-state IL electrolyte, which provides a wider voltage window, is evidenced when comparing the energy density of printed µcup-MSCs to other solution-processed non-MXene MSCs, such as rGO,[47] spray coated graphene,[48] poly(3,4-ethylenedioxythiophene) polystyrene sulfonate–graphene (PEDOT-G),[48] and MnO$_2$-graphene quantum dots (GQD)[49] based MSCs, etc. (Figure 5H). The power density is also much higher for the non-MXene MSCs except PEDOT-Ag, indicating a high rate-response in the µcup-MSCs. The energy density

and power density of the printed µcup-MSCs can be further improved by either optimizing the µcups design, matching two electrodes, engineering MXene surface chemistries, and/or enhancing the wettability of IL electrolyte toward graphene/MXene electrodes, etc. The rich family of MXenes also offers great opportunities to achieve superior MSCs based on MXenes other than Ti$_3$C$_2$T$_x$.

3. Conclusion

In summary, a novel MSC configuration that combines a sandwiched (on device scale) and interdigitated (locally) electrode structure by fabricating a µcup electrode was demonstrated. Such a new architecture facilitates ion diffusion, allows for a reduced amount of electrolyte, and increases the utilization of active materials, best evidenced by two µcups designs, one by laser-scribing and the other by direct screen printing. Even though difficult to quantify, the fabricated solid-state µcup-MSCs demonstrate improved charge storage performance, including volumetric capacitance and excellent cycling performance over the flat sandwich geometry. But most importantly, this architecture allows the printing of asymmetric devices with high lateral resolution. This is difficult with interdigitated electrodes as the second electrode finger needs to be placed with high accuracy between the fingers of the first electrode. We here only presented a first proof-of-concept, it is reasonable to assume that with further optimization the charge storage properties of µcup-MSCs can be substantially enhanced.

4. Experimental Section

Experimental details, including laser scribing, graphene synthesis, MAX etching, MXene delamination, solution processing of the devices, and their characterizations, are provided in the Supporting Information.

Supporting Information

Supporting Information is available from the Wiley Online Library or from the author.

Conflict of interest

The authors declare no conflict of interest.

Data Availability Statement

Keywords

[1] P. Simon, Y. Gogotsi, *Nat. Mater.* **2020**, *19*, 1151.

[2] M. Beidaghi, Y. Gogotsi, *Energy Environ. Sci.* **2014**, *7*, 867.

[3] W. Tian, A. VahidMohammadi, M. S. Reid, Z. Wang, L. Ouyang, J. Erlandsson, T. Pettersson, L. Wågberg, M. Beidaghi, M. M. Hamedi, W. Tian, M. S. Reid, Z. Wang, L. Ouyang, J. Erlandsson, T. Pettersson, L. Wågberg, M. M. Hamedi, A. VahidMohammadi, M. Beidaghi, *Adv. Mater.* **2019**, *31*, 1902977.

[4] S. Abdolhosseinzadeh, J. Heier, C. Zhang, *ChemElectroChem* **2021**, *8*, 1911.

[5] S. Abdolhosseinzadeh, J. Heier, C. Zhang, *J. Phys. Energy* **2020**, *2*, 031004.

[6] L. Zhang, H. Liu, Y. Zhao, X. Sun, Y. Wen, Y. Guo, X. Gao, C. A. Di, G. Yu, Y. Liu, *Adv. Mater.* **2012**, *24*, 436.

[7] Y. Y. Peng, B. Akuzum, N. Kurra, M. Q. Zhao, M. Alhabeb, B. Anasori, E. C. Kumbur, H. N. Alshareef, M. Der Ger, Y. Gogotsi, *Energy Environ. Sci.* **2016**, *9*, 2847.

[8] M. F. El-Kady, V. Strong, S. Dubin, R. B. Kaner, *Science* **2012**, *335*, 1326.

[9] X. Wang, V. Raju, W. Luo, B. Wang, W. F. Stickle, X. Ji, *J. Mater. Chem. A* **2014**, *2*, 2901.

[10] D. Qi, Y. Liu, Z. Liu, L. Zhang, X. Chen, D. Qi, Y. Liu, Z. Liu, L. Zhang, X. Chen, *Adv. Mater.* **2017**, *29*, 1602802.

[11] H. Li, J. Liang, H. Li, J. Liang, *Adv. Mater.* **2020**, *32*, 1805864.

[12] J. Liang, C. Jiang, W. Wu, *Appl. Phys. Rev.* **2021**, *8*, 021319.

[13] Y. Shao, M. F. El-Kady, J. Sun, Y. Li, Q. Zhang, M. Zhu, H. Wang, B. Dunn, R. B. Kaner, *Chem. Rev.* **2018**, *118*, 9233.

[14] S. Najib, E. Erdem, *Nanoscale Adv* **2019**, *1*, 2817.

[15] L. Liu, Z. Niu, J. Chen, *Chinese Chem. Lett.* **2018**, *29*, 571.

[16] L. Hu, H. Wu, Y. Cui, *Appl. Phys. Lett.* **2010**, *96*, 183502.

[17] Y. Wang, Y. Z. Zhang, D. Dubbink, J. E. ten Elshof, *Nano Energy* **2018**, *49*, 481.

[18] C. (John) J. Zhang, S. H. Park, S. E. O'Brien, A. Seral-Ascaso, M. Liang, D. Hanlon, D. Krishnan, A. Crossley, N. McEvoy, J. N. Coleman, V. Nicolosi, *Nano Energy* **2017**, *39*, 151.

[19] S. Xu, Y. Dall'Agnese, G. Wei, C. Zhang, Y. Gogotsi, W. Han, *Nano Energy* **2018**, *50*, 479.

[20] Y. D. Kim, J. Hone, *Nature* **2017**, *544*, 167.

[21] J. Li, S. Sollami Delekta, P. Zhang, S. Yang, M. R. Lohe, X. Zhuang, X. Feng, M. Östling, *ACS Nano* **2017**, *11*, 8249.

[22] F. Torrisi, T. Hasan, W. Wu, Z. Sun, A. Lombardo, T. S. Kulmala, G. W. Hsieh, S. Jung, F. Bonaccorso, P. J. Paul, D. Chu, A. C. Ferrari, *ACS Nano* **2012**, *6*, 2992.

[23] C. Yuning Meng, Y. Zhao, C. Hu, H. Cheng, Y. Hu, Z. Zhang, G. Shi, L. Qu, Y. Meng, Y. Zhao, C. Hu, H. Cheng, Z. Zhang, L. Qu, G. Shi, *Adv. Mater.* **2013**, *25*, 2326.

[24] X. Shi, S. Pei, F. Zhou, W. Ren, H. M. Cheng, Z. S. Wu, X. Bao, *Energy Environ. Sci.* **2019**, *12*, 1534.

[25] J. M. Munuera, J. I. Paredes, M. Enterría, S. Villar-Rodil, A. G. Kelly, Y. Nalawade, J. N. Coleman, T. Rojo, N. Ortiz-Vitoriano, A. Martínez-Alonso, J. M. D. Tascón, *ACS Appl. Mater. Interfaces* **2020**, *12*, 494.

[26] Q. Chang, L. Li, L. Sai, W. Shi, L. Huang, *Adv. Electron. Mater.* **2018**, *4*, 1800059.

[27] C. Zhang, Y. Ma, X. Zhang, S. Abdolhosseinzadeh, H. Sheng, W. Lan, A. Pakdel, J. Heier, F. Nüesch, *Energy Environ. Mater.* **2020**, *3*, 29.

[28] M. Vural, A. Pena-Francesch, J. Bars-Pomes, H. Jung, H. Gudapati, C. B. Hatter, B. D. Allen, B. Anasori, I. T. Ozbolat, Y. Gogotsi, M. C. Demirel, M. Vural, A. Pena-Francesch, J. Bars-Pomes, H. Jung, H. Gudapati, I. T. Ozbolat, M. C. Demirel, C. B. Hatter, B. Anasori, Y. Gogotsi, B. D. Allen, *Adv. Funct. Mater.* **2018**, *28*, 1801972.

[29] X. Jiang, W. Li, T. Hai, R. Yue, Z. Chen, C. Lao, Y. Ge, G. Xie, Q. Wen, H. Zhang, *npj 2D Mater. Appl.* **2019**, *3*, 34.

[30] C. (John) Zhang, L. McKeon, M. P. Kremer, S. H. Park, O. Ronan, A. Seral-Ascaso, S. Barwich, C. Coileáin, N. McEvoy, H. C. Nerl, B. Anasori, J. N. Coleman, Y. Gogotsi, V. Nicolosi, *Nat. Commun.* **2019**, *10*, 1795.

[31] C. Zhang, M. P. Kremer, A. Seral-Ascaso, S.-H. Park, N. McEvoy, B. Anasori, Y. Gogotsi, V. Nicolosi, C. F. Zhang, M. P. Kremer, A. Seral-Ascaso, S. Park, N. McEvoy, V. Nicolosi, B. Anasori, Y. Gogotsi, *Adv. Funct. Mater.* **2018**, *28*, 1705506.

[32] J. Zhang, N. Kong, S. Uzun, A. Levitt, S. Seyedin, P. A. Lynch, S. Qin, M. Han, W. Yang, J. Liu, X. Wang, Y. Gogotsi, J. M. Razal, J. Zhang, S. Seyedin, P. A. Lynch, S. Qin, X. Wang, J. M. Razal, N. Kong, W. Yang, S. Uzun, A. Levitt, M. Han, Y. A. Gogotsi, J. Liu, *Adv. Mater.* **2020**, *32*, 2001093.

[33] X. Zhao, D. E. Holta, Z. Tan, J. H. Oh, I. J. Echols, M. Anas, H. Cao, J. L. Lutkenhaus, M. Radovic, M. J. Green, *ACS Appl. Nano Mater.* **2020**, *3*, 10578.

[34] M. Alhabeb, K. Maleski, B. Anasori, P. Lelyukh, L. Clark, S. Sin, Y. Gogotsi, *Chem. Mater.* **2017**, *29*, 7633.

[35] C. J. Zhang, S. Pinilla, N. McEvoy, C. P. Cullen, B. Anasori, E. Long, S. H. Park, A. Seral-Ascaso, A. Shmeliov, D. Krishnan, C. Morant, X. Liu, G. S. Duesberg, Y. Gogotsi, V. Nicolosi, *Chem. Mater.* **2017**, *29*, 4848.

[36] S. Abdolhosseinzadeh, R. Schneider, A. Verma, J. Heier, F. Nüesch, C. Zhang, S. Abdolhosseinzadeh, R. Schneider, A. Verma, J. Heier, F. Nüesch, C. Zhang, *Adv. Mater.* **2020**, *32*, 2000716.

[37] V. Paolucci, G. D'Olimpio, L. Lozzi, A. M. Mio, L. Ottaviano, M. Nardone, G. Nicotra, P. Le-Cornec, C. Cantalini, A. Politano, *ACS Sustainable Chem. Eng.* **2020**, *8*, 18830.

[38] L. G. Cançado, A. Jorio, E. H. M. Ferreira, F. Stavale, C. A. Achete, R. B. Capaz, M. V. O. Moutinho, A. Lombardo, T. S. Kulmala, A. C. Ferrari, *Nano Lett.* **2011**, *11*, 3190.

[39] C. C. Yang, H. Y. Lin, A. Kumar, B. Pattanayak, H. Y. Tsai, T. Winie, T. Y. Tseng, *RSC Adv.* **2018**, *8*, 30239.

[40] C. Zhang, B. Anasori, A. Seral-Ascaso, S.-H. Park, N. McEvoy, A. Shmeliov, G. S. Duesberg, J. N. Coleman, Y. Gogotsi, V. Nicolosi, C. F. Zhang, A. Seral-Ascaso, S. Park, N. McEvoy, A. Shmeliov, J. N. Coleman, V. Nicolosi, G. S. Duesberg, B. Anasori, Y. Gogotsi, *Adv. Mater.* **2017**, *29*, 1702678.

[41] C. Couly, M. Alhabeb, K. L. Van Aken, N. Kurra, L. Gomes, A. M. Navarro-Suárez, B. Anasori, H. N. Alshareef, Y. Gogotsi, *Adv. Electron. Mater.* **2018**, *4*, 1700339.

[42] Z. Lin, P. Rozier, B. Duployer, P. L. Taberna, B. Anasori, Y. Gogotsi, P. Simon, *Electrochem. Commun.* **2016**, *72*, 50.

[43] Z. Lin, D. Barbara, P. L. Taberna, K. L. Van Aken, B. Anasori, Y. Gogotsi, P. Simon, *J. Power Sources* **2016**, *326*, 575.

[44] T. M. Higgins, J. N. Coleman, *ACS Appl. Mater. Interfaces* **2015**, *7*, 16495.

[45] C. (John) Zhang, T. M. Higgins, S. H. Park, S. E. O'Brien, D. Long, J. N. Coleman, V. Nicolosi, *Nano Energy* **2016**, *28*, 495.

[46] Y. Zhu, S. Wang, J. Ma, P. Das, S. Zheng, Z. S. Wu, *Energy Storage Mater.* **2022**, *51*, 500.

[47] J. J. Yoo, K. Balakrishnan, J. Huang, V. Meunier, B. G. Sumpter, A. Srivastava, M. Conway, A. L. Mohana Reddy, J. Yu, R. Vajtai, P. M. Ajayan, *Nano Lett.* **2011**, *11*, 1423.

[48] H. Li, Y. Hou, F. Wang, M. R. Lohe, X. Zhuang, L. Niu, X. Feng, H. Li, Y. Hou, F. Wang, M. R. Lohe, X. Zhuang, X. Feng, L. Niu, X. Zhuang Shanghai Key, *Adv. Energy Mater.* **2017**, *7*, 1601847.

[49] W. W. Liu, Y. Q. Feng, X. Bin Yan, J. T. Chen, Q. J. Xue, *Adv. Funct. Mater.* **2013**, *23*, 4111.

2300357 (10 of 10)